http://dx.doi.org/10.5012/bkcs.2014.35.10.3111

Structural and Luminescence Properties of 6-Oxo-5-phenyl-6*H*-pyrido[3,2,1-*jk*]carbazol-4-yl thiophene-2-carboxylate

Yong-Kwang Jeong, Min-Ah Kim, Hyo-Sung Lee, Sung Woo Lee,† and Jun-Gill Kang*

*Department of Chemistry, Chungnam National University, Daejeon 305-764, Korea. *E-mail: jgkang@cnu.ac.kr*
†Center for Research Facilities, Chungnam National University, Yuseong-gu, Daejeon 305-764, Korea
Received March 28, 2014, Accepted June 18, 2014

Key Words : Pyridocarbazone, Structure, Luminescence, Proton-substitution effect, Quantum mechanical calculation

Pyrido[3,2,1-*jk*]carbazol-6-one (PCO) derivatives are very attractive as new materials in organoelectronics and photophysical applications, because of their planar structure with rich π-electron section. Most studies on PCO derivatives have examined their synthesis and reactions.[1-4] Previously, we synthesized 4-hydroxy-5-phenyl-6*H*-pyrido[3,2,1-*jk*]-carbazol-6-one (HPPCO) derivatives and investigated their luminescence properties.[5] HPPCO exposed to UV light produced deep-blue to green luminescence, depending on the solvent. The solvatochromic effect was strongly associated with the degree of the deprotonation of the hydroxyl group substituted to the fused ring. When the proton of 4-hydorxy was substituted by acetate (6-oxo-5-phenyl-6*H*-pyrido[3,2,1-*jk*]carbazol-4-yl acetate, OPPCA) or benzoate (6-oxo-5-phenyl-6*H*-pyrido[3,2,1-*jk*]carbazol-4-yl benzoate, OPPCB), those compounds did not exhibit any solvatochromic effect with the emission peaking at 415 nm. In this study we synthesized 6-oxo-5-phenyl-6*H*-pyrido [3,2,1-*jk*] carbazol-4-yl thiophene-2-carboxylate (OPPCT), and investigated the structural and luminescence properties as a series of PCO derivatives.

OPPCT crystallized in the monoclinic space group $P2_1/c$ with a = 8.6431(11) Å, b = 35.860(5) Å, c = 6.7100(8) Å, β = 111.150(7)°, V = 1939.6(4) Å^3, and Z = 4. Prospective view of OPPCT with the atomic numbering scheme is shown in Figure 1(a), and the geometric parameters are listed in Table S1 (Supporting Information). The PCO fused ring was characterized by the least-squares plane of the – 4.5725(0.0056) x + 0.0103(0.0185) y + 6.5914(0.0013) z = 0.2926(0.0064) with a root-mean-square deviation of 0.0481 Å. The average dihedral angle between the main frame and the substituted ring was 60.98(0.13)° for the phenyl ring and 74.69(0.16)° for the thiophene ring. There was no classical hydrogen bond resulted from OH in the three-dimensional arrangements of OPPCT. However, the shortest intermolecular distance between the carbon atom (C19) as a donor (D) and the oxygen atom (O3) of the carbonyl group as an acceptor (A) was 3.360 Å, and the next shortest distance, d(D···A) was 3.421 Å between C6 and O1. These D···A distances are classified as a weak electrostatic interaction.[6,7] Comparably, the intermolecular hydrogen bond formed by O3 in the substituted thiophene carboxylate group played a key role on forming the crystal network, as shown in Figure 1(b).

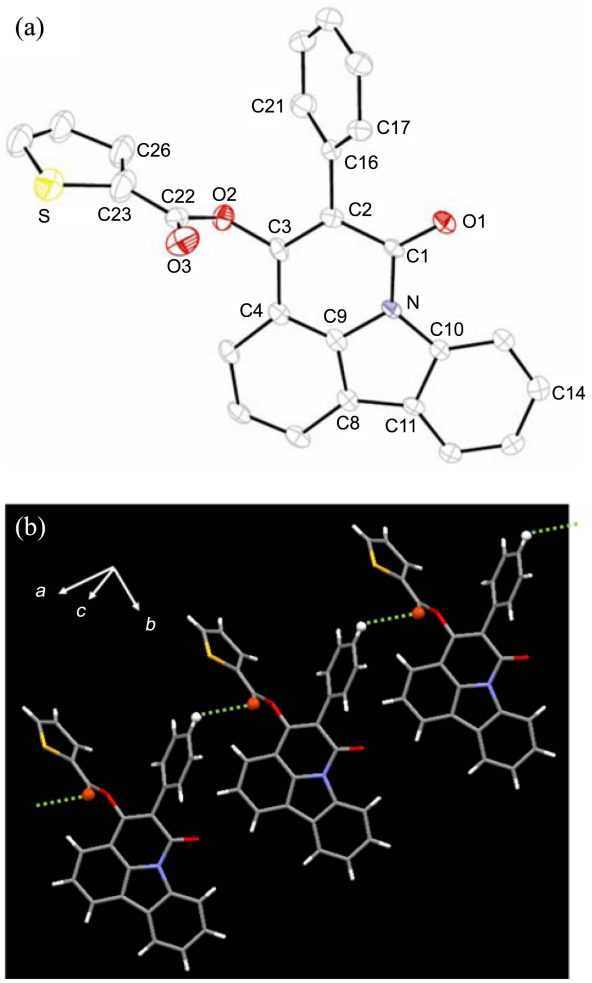

Figure 1. (a) Prospective view of OPPCT showing atomic labeling and ellipsoid at 50%, and (b) part of the hydrogen-bonded framework of OPPCT.

Figure 2 shows the absorption spectra of HPPCO and its derivatives dissolved in dichloromethane (DCM). The absorption spectrum of HPPCO in the 280–450 nm region consisted of the three A-band components, peaking at 369, 353 and 339 nm (these components are referred to as A1, A2

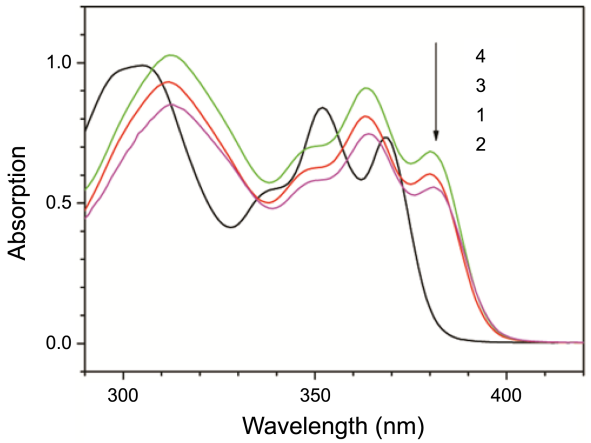

Figure 2. Absorption spectra of HPPCO (1) and its derivatives (2: OPPCT, 3: OPPCA and 4: OPPCB) dissolved in DCM (6×10^{-5} M).

and A3 in order of increasing energy), and the B-band, peaking at 302 nm. There was no significant difference in the intensity and the spectral structure between HPPCO and its derivatives except the redshift by ~10 nm due to the proton substitution. These results indicated that the A- and B-absorption bands were associated with the electronic transitions of the fused ring. Figure 3 shows the emission and the excitation spectra of HPPCO and OPPCT dissolved in DCM. Taking into account the approximately 10-nm redshift, the spectral shapes of the emission and the excitation spectra of OPPCT were very similar to those of HPPCO. However, the emission intensity of OPPCT was much stronger than that of HPPCO. The emission spectra of HPPCO and OPPCT resolved into three main components with a low-energy shoulder: 416, 397 and 380 nm for HPPCO, and 433, 414 and 402 nm for OPPCT as inserted in Figure 3. The A1, A2 and A3 excited states were responsible for these three components, respectively. The low-energy shoulder was assigned as the phosphorescence component. The excitation spectrum of the blue emission from OPPCT were also consisted of the three main component (386, 369 and 340 nm) with a high-energy shoulder (301 nm). The three main

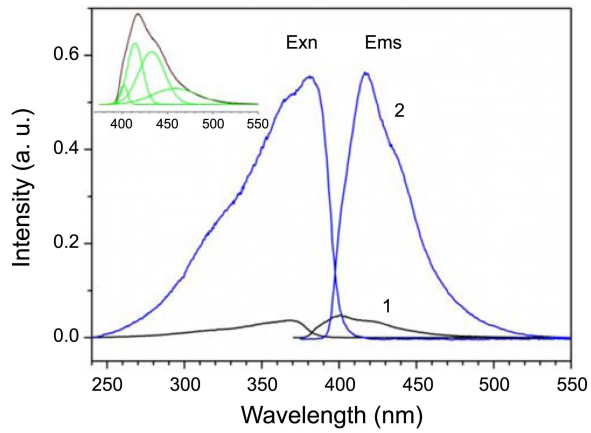

Figure 3. Emission and excitation spectra of HPPCO (1) and OPPCT (2) dissolved in DCM (5×10^{-5} M).

Table 1. Luminescence Properties of HPPCO and OPPCT dissolved in DCM

	λ_{ems}/nm			Φ/%	τ/ns	$k/10^7$ s^{-1}	
	A1	A2	A3			k_r	k_{nr}
HPPCO	416	397	380	2.7	4.2	0.64	230
OPPCT	433	414	402[a]	14.0	5.5	2.6	160

[a]very weak

components corresponded to the A1 and A2 and A3-absorption bands, respectively; and the high-energy shoulder represented the B-absorption band. The quantum yield and the decay time of the blue luminescence of OPPCT dissolved in DCM were measured, and the results were compared with those of HPPCO in Table 1. The quantum yield of OPPCT (Φ = 14.0%) was more than five times as much as that of HPPCO (Φ = 2.7%), whereas the observed decay time of OPPCT (τ = 5.5 ns) was slightly longer than that of HPPCO (τ = 4.2 ns). The quantum yield of the luminescence, defined as the ratio of the number of photons emitted to the number of photons absorbed, also reveals how well the radiative processes compete with non-radiative processes. A general expression for the quantum yield in terms of rate constant is

$$\Phi = \frac{k_r}{k_r + k_{nr}}$$

where k_r and k_{nr} are the rate constants for the radiative and the non-radiative processes, respectively. Since $\tau = (k_r + k_{nr})^{-1}$, the radiative and the non-radiative rate constants are expressed by:

$$k_r = \frac{\Phi}{\tau}$$

$$k_{nr} = \frac{1 - \Phi}{\tau}$$

As listed in Table 1, for OPPCT, the radiative rate-constant was four times as much as that for HPPCO. These results supported that the proton substitution significantly reduced the energy-loss process associated with the OH group and consequently enhanced the luminescence efficiency.

Theoretical calculations for electronic structures and electronic transitions of OPPCT molecule were also performed to interpret the observed optical properties. The structure was initially optimized using DFT-B3LYP/6-31g(d,p) basis set.[8] The comparison of geometric parameters determined from the experimental (X-ray) and the optimized structures is given in Table S1 (Supporting Information). The standard deviation between the experimental and the calculated values is 0.0164 Å for the bond lengths and 2.39° for the bond angles. The large differences were found in the bond angles forming from at least two of C3, O2, O3, C22 and C23 atoms. It was due that the crystal packing effect was not accounted in the geometry optimization of the single molecule. Next, a Configuration Interaction Singles (CIS) calculation was performed with ZINDO method[8] on the basis of

the optimized geometry. The results for molecular orbitals and electronic structures are listed in Tables S2 and S3, respectively. Comparing the calculated wavelengths with the observed absorption-band positions, the calculated excited states were classified into three groups as listed in Table S3. Among the excited states in group A, the transitions from the X state to the 1A, 2A and 4A states have moderate oscillator strengths with f = 0.272, 0.152 and 0.235, respectively, while the X → 3A transitions have lower oscillator-strength with f = 0.012. The first excited state, 1A, arose predominantly from the transition from the highest occupied molecular orbital (HOMO), h1, to the lowest unoccupied molecular orbital (LUMO), l1. As shown in Figure 3, the h1 HOMO comprised a combination of the p_z orbitals of carbon atoms in ring 3 (C4 – C9) and ring 4 (C1 – N) of the fused ring, the p_x and p_y orbitals of the carbon atoms in the phenyl ring (ph), and the p_z orbital of O1. Note that the molecular axis is represented by the z-axis. The contributions of the fused ring, the phenyl ring and the oxygen atom were 56%, 31% and 9%, respectively. Accordingly, the h1 HOMO was characterized as the π orbital locating over rings 3 and 4, the oxygen atom of the carbonyl group, and the phenyl ring, hereafter, referred to as π(R3,4;O1;ph). As shown in Figure 3, the l1 LUMO was contributed from the π* orbital located on ring 2 (C8 – C11) – ring 4 of the fused ring (66%) as main and the π* orbital located on the thiophene ring (thio, 18%) as minor. These contributions specified the l1 LUMO as π*(R2-4;thio). Accordingly, the A1-absorption component can be assigned as π(R3,4;O1;ph) → π*(R2-4;thio). The second excited state, 2A, is predominantly a result of the transitions from the h8 HOMO to the l1 LUMO. The h8 HOMO was contributed from the p_x, p_y and p_z orbitals of O1, of which the contributions were 70%, 4% and 3%, respectively. Thus, the h8 HOMO was characterized as n(O1). Another transition, contributed to the 2A excited state, was the h8 → l4 transition. The l4 LUMO corresponded to the π* orbital locating over rings 3 and 4, π*(R3,4), because their contributions were more than 80%. The X → 2A transition was responsible for the A2-absorption component. The 4A excited state (f = 0.235) was resulted from the h2 → l1 transition. The next HOMO, h2, corresponded to π(R1-3), locating over the carbon atoms in rings 1, 2 and 3 (> 97%). Accordingly, the X → 4A transition was responsible for the A3-absorption component, assigned as π(R1-3) → π*(R2-4;thio). The electron density isocontours responsible for the A1, A2 and A3-absorption components are shown in Figure 3.

In summary, when exposed to UV light, HPPCO and its derivative OPPCT produced deep-blue and blue-green luminescence, respectively. The proton substitution increased the luminescence quantum-yield by more than five-fold, due to the reduction of the energy-loss by the hydroxyl group. DFT and ZINDO calculations on the structural and the optical properties showed that the luminescence was strongly associated with the π → π* transitions of the fused ring with a minor contribution coming from the phenyl ring and the oxygen atom of the carbonyl group. The substituted thiophene carboxylate group played a key role on forming the crystal network.

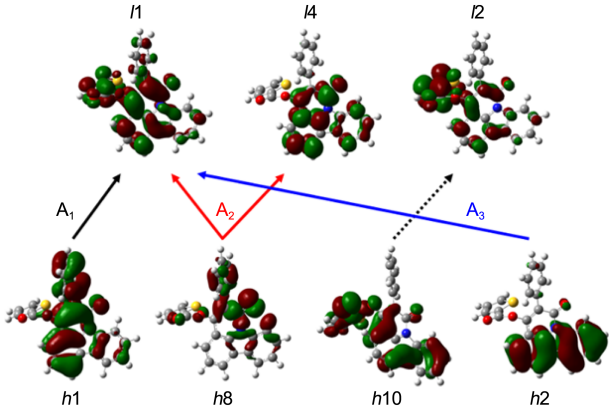

Figure 3. Electron density isocontours of some HOMOs and LUMOs involved in the A-band transitions of OPPCT.

Experimental

Synthesis of OPPCT. HPPCO was synthesized from carbazole (8.35 g, 0.05 mol) and diethyl phenylmalonate (14.15 g, 0.06 mol) according to Method A described in Ref. 1. A mixture of HPPCO (3.1 g, 10 mmol) and potassium carbonate (1.38 g, 10 mmol) was dissolved in acetone (300 mL). To the greenish acetone solution, 2-thiophenecarbonyl chloride (1.61 g, 11 mmol) was added and stirred at room temperature for 3 h. The orange powder was filtered and then dissolved in a 1:1 chloroform and water mixed solvent (200 mL). The organic phase was separated and dried over anhydrous magnesium sulfate. The precipitate was obtained by evaporating the solvent and then was washed several times with hexane. ^{1}H NMR ($CDCl_3$) δ 1H, d, 8.73 (J = 8 Hz), 1H, d, 8.16 (J = 8 Hz), 1H, d, 8.08 (J = 8 Hz), 1H, d, 7.87 (J = 4 Hz), 1H, d, 7.68 (J = 8 Hz), 1H, d, 7.66 (J = 4 Hz), 1H, t, 7.59 (J = 8 Hz), 4H, m, 7.55-7.51, 1H, t, 7.50 (J = 8 Hz), 2H, t, 7.38 (J = 8 Hz), 1H, t, 7.31 (J = 8 Hz), 1H, d, 7.13 (J = 4 Hz). Anal. found: C, 72.7; H, 3.3; N, 3.7; O, 12.2; S, 6.6. Calcd. for $C_{26}H_{15}NO_3S$: C, 74.1; H, 3.6; N, 3.3; O, 11.4; S, 7.6.

X-ray Crystallograpy. Single crystals of OPPCT were grown from dichloromethane solution using the slow-evaporation method. Diffraction data were collected at room temperature on a Bruker SMART CCD diffractometer using graphite monochromated Mo Kα radiation. The structure was solved by applying the direct method using SHELXS-97 and refined by a full-matrix least-squares calculation on F^2 using SHELXL-97.[9] All non-H atoms were refined with anisotropic displacement parameters. Hydrogen atoms were fixed at ideal geometric positions, and their contributions were included in the structural factor calculations. The crystal data and refinement results are listed in Table S4. Crystallographic data for the structure reported here have been deposited with CCDC (Deposition No. CCDC-993939). These data can be obtained free of charge *via* http://www.ccdc.cam.ac.uk/conts/retrieving.html or from CCDC, 12 Union Road, Cambridge CB2 1EZ, UK, E-mail:

deposit@ccdc.cam.ac.uk.

Optical Measurements. The absorption spectra, the luminescence and the excitation spectra, the luminescence quantum yield, and the luminescence decay time were measured using previously described methods.[5]

Acknowledgments. This research was supported by National Research Foundation (NRF-2012R1A1A2007201).

Supporting Information. Geometric parameters from X-ray data and optimized calculation (Table S1), molecular orbitals (Table S2), details of CIS excited states (Table S3), and crystal data and refinement (Table S4) are included in supporting information.

References

1. Dang, H. V.; Knobloch, B.; Habib, N. S.; Kappe, T.; Stadlbauer, W. *J. Heterocyclic Chem*. **2005**, *42*, 85.
2. Dang, H. V.; Stadlbauer, W. *J. Heterocyclic Chem*. **2006**, *43*, 65.
3. Shivachev, B.; Petrov, P.; Stoyanova, M. *J. Chem. Crystallogr*. **2009**, *39*, 209.
4. Stadlbauer, W.; Dang, H. V.; Knobloch, B. W. *J. Heterocyclic Chem.* **2011**, *48*, 1039.
5. Lee, H.-S.; Kim, H.-J.; Kang, J.-G. *Photochem. Photobio. Sci.* **2011**, *10*, 1338.
6. Jeffrey, G. A. *An Introduction to Hydrogen Bonding*; Oxford University Press: New York, 1997; Chapters 2 and 5.
7. Steiner, T; Saenger, W. *J. Am. Chem. Soc*. **1992**, *114*, 10146.
8. Frisch, M. J. T.; Trucks, G. W.; Schlegel, H. B.; Scuseria, G. E.; Robb, M. A.; Cheeseman, J. R.; Scalmani, G.; Barone, V.; Mennucci, B.; Petersson, G. A.; Nakatsuji, H.; Caricato, M.; Li, X.; Hratchian, H. P.; Izmaylov, A. F.; Bloino, J.; Zheng, G.; Sonnenberg, J. L.; Hada, M.; Ehara, M.; Toyota, K.; Fukuda, R.; Hasegawa, J.; Ishida, M.; Nakajima, T.; Honda, Y.; Kitao, O.; Nakai, H.; Vreven, T.; Montgomery, J. A., Jr.; Peralta, J. E.; Ogliaro, F.; Bearpark, M.; Heyd, J. J.; Brothers, E.; Kudin, K. N.; Staroverov, V. N.; Kobayashi, R.; Normand, J.; Raghavachari, K.; Rendell, A.; Burant, J. C.; Iyengar, S. S.; Tomasi, J.; Cossi, M.; Rega, N.; Millam, N. J.; Klene, M.; Knox, J. E.; Cross, J. B.; Bakken, V.; Adamo, C.; Jaramillo, J.; Gomperts, R.; Stratmann, R. E.; Yazyev, O.; Austin, A. J.; Cammi, R.; Pomelli, C.; Ochterski, J. W.; Martin, R. L.; Morokuma, K.; Zakrzewski, V. G.; Voth, G. A.; Salvador, P.; Dannenberg, J. J.; Dapprich, S.; Daniels, A. D.; Farkas, Ö.; Foresman, J. B.; Ortiz, J. V.; Cioslowski, J.; Fox, D. J. *Gaussian 09* (Revision A. 02); Gaussian, Inc., Wallingford CT, 2009.
9. Sheldrick, G. M. *Acta Crystallogr. A* **2008**, *64*, 112.